

UNIVERSITÀ POLITECNICA DELLE MARCHE
Repository ISTITUZIONALE

Calibration of Scanning Microwave Microscopy via Substrate-Referenced Machine Learning

This is the peer reviewd version of the followng article:

Original
Calibration of Scanning Microwave Microscopy via Substrate-Referenced Machine Learning / Zhang, Y., Wang, X., Farina, M., Hwang, J.C.M., Zhu, Y., Mao, N., Wu, P., Kong, J.. - (2026). (107th ARFTG Microwave Measurement Conference, ARFTG 2026 Boston, USA 12 June 2026) [10.1109/ARFTG68740.2026.11614661].

Availability:
This version is available at: 11566/364474 since: 2026-10-13T17:09:48Z

Publisher:
Institute of Electrical and Electronics Engineers Inc.

Published
DOI:10.1109/ARFTG68740.2026.11614661

Terms of use:

The terms and conditions for the reuse of this version of the manuscript are specified in the publishing policy. The use of copyrighted works requires the consent of the rights' holder (author or publisher). Works made available under a Creative Commons license or a Publisher's custom-made license can be used according to the terms and conditions contained therein. See editor's website for further information and terms and conditions.
This item was downloaded from IRIS Università Politecnica delle Marche (https://iris.univpm.it). When citing, please refer to the published version.

Publisher copyright:

IEEE - Postprint/Author's Accepted Manuscript

©2026 IEEE. Personal use of this material is permitted. Permission from IEEE must be obtained for all other uses, in any current or future media, including reprinting/republishing this material for advertising or promotional purposes, creating new collective works, for resale or redistribution to servers or lists, or reuse of any copyrighted component of this work in other works. To access the final edited and published work see 10.1109/ARFTG68740.2026.11614661

(Article begins on next page)

02 November 2026

Calibration of Scanning Microwave Microscopy via Substrate-referenced Machine Learning

Yawei Zhang[1], Xiaopeng Wang[1], Marco Farina[1,3], James C.M. Hwang[1], Yunyue Zhu[2], Nannan Mao[2], Peng Wu[2], Jing Kong[2]
[1]Cornell University, Ithaca, NY, USA
[2]Massachusetts Institute of Technology, Cambridge, MA, USA
[3]Universita Politecnica delle Marche, Ancona, Italy

***Abstract*—Scanning microwave microscopy (SMM) utilizes near-field microwave radiation to offer unparalleled nanoscale material characterization; yet its widespread adoption is hindered by the sophisticated nature of the manual one-port calibration process. Solving this inverse problem is complicated and prohibitive for real-time use. Furthermore, manual calibration often fails to accurately track dynamic changes in probe tip geometry, which is a critical factor in near-field interaction and can result in persistent measurement uncertainty and operator-dependent errors. To overcome these barriers, this work introduces a substrate-referenced deep learning (DL) framework that automates the solution to this inverse problem. By decoupling static substrate parasitics from dynamic tip geometry, a TabPFN-based regressor chain with a root-mean-square error (RMSE) of 0.0086 infers error factors due to the effective probe shapes from a single approach curve, combining with an error correction factor from static substrate parasitics to realize real-time calibration, which greatly reduces calibration times by orders of magnitude and eliminates human variability, enabling real-time, quantitative SMM imaging that was previously unattainable. This method was validated on 2D tin selenide (SnSe) samples with various thicknesses on SiO_2/Si^{++} and Si++ substrates, demonstrating accuracy comparable to expert manual calibration and reducing processing time from hours to seconds, transforming SMM into an accessible tool for the broader research community.**

***Keywords*—Atomic force microscopy (AFM), calibration, machine learning, tin selenide, two-dimensional materials, scanning microwave microscopy (SMM)**

I. Introduction

With the fast growth of nanotechnology and two-dimensional (2D) material research, it has been challenging to use conventional material characterization techniques to determine the structural or electrical properties of 2D materials. Scanning microwave microscopy has been gaining attention within these research areas, as it has emerged as a critical tool bridging the gap between microwave engineering and nanotechnology. By combining the spatial resolution of atomic force microscopy (AFM) with the electrical sensitivity of a vector network analyzer (VNA), SMM offers unparalleled capabilities for the non-destructive subsurface characterization of complex material systems, including the characterization of semiconductors, dielectrics, and biological cells [1] - [11] . However, despite its great potential, the widespread adoption of SMM beyond specialized laboratories is severely stifled by the complexity of the calibration process.

In standard practice, the measured signal is a convolution of the material's properties response, the parasitics from setups, the topographic variations of the sample surface, and the geometric factors of the scanning probe and cantilevers. Furthermore, the solution to this near-field electromagnetic inverse calibration problem is heavily dependent on the precise geometry of the probe tip. The manual analytical process typically approximates the tip's geometry and assumes consistency after a few times of scanning, leading to persistent operator-dependent errors and measurement uncertainty.

To resolve these issues, this work presents a substrate-referenced machine learning calibration framework that automates the solution to the SMM calibration inverse problem. We propose a split-calibration architecture that decouples the calibration into two distinct components: a static substrate-specific baseline that can be derived from the substrate-specific parasitic contributions and a dynamic tip geometry factor, which can be inferred in real-time by a TabPFN-based regressor. The training dataset includes all experimental data and uses physics-informed domain randomization for training dataset augmentation.

This hybrid approach allows for the instantaneous extraction of effective probe geometry from a single pre-experimental approach curve. As long as the substrate on which the sample mounted is collected in the library of our model, we can calibrate in real time and imaging material properties in real time, thereby transforming SMM into an accessible, high-throughput tool for the broader materials community.

II. Method

A. SnSe Sample

2D SnSe flakes are synthesized using low-pressure physical vapor deposition [12]. The synthesis begins by placing SnSe powder precursor in a crucible at the center of a tube furnace. A freshly exfoliated mica substrate, annealed at 400 °C in air for 10 min, is positioned 10-cm downstream from the precursor. The furnace is then evacuated to 10 mTorr and heated to 420 °C for a deposition of approximately 40 min. After deposition, the furnace is quickly cooled to room

temperature [12]. Finally, SnSe flakes are transferred using polymethyl methacrylate (PMMA) from mica to three different substrates: bare SnSe samples on a doped 20um Si substrate precoated with 300-nm-thick SiO_2 and directly on a doped Si substrate, or SnSe sample on SiO_2/Si^{++} substrate. The synthesized SnSe flakes are up to 23-μm wide with a thickness of 2 to 175.25 nm. Note that the region between the flakes where the Si substrate is exposed can be used for SMM calibration.

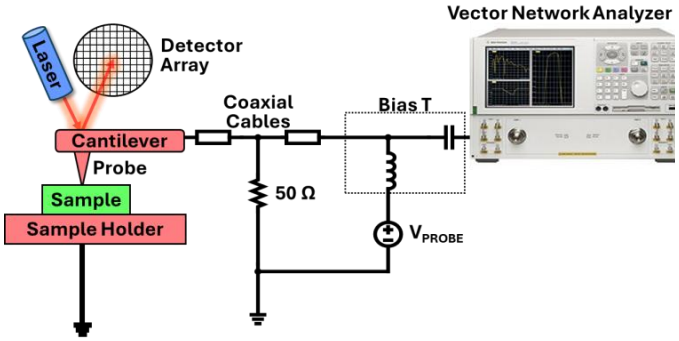


Fig. 1. Schematics of the AFM-based SMM.

B. SMM Setup

Fig. 1. illustrates the SMM/AFM setup. It is based on a Keysight Technologies 7500 AFM equipped with an N9545C SMM nose cone [9]. A Rocky Mountain 25Pt300A platinum probe, featuring a spring constant of 18 N/m and a tip radius of 25 nm, serves as the dual-function AFM/SMM probe. This probe is affixed to a platinum cantilever 300-μm long, 60-μm wide, and 2-μm thick. The cantilever is connected to a Keysight Technologies E8062B vector network analyzer (VNA) via coaxial cables. For impedance matching around 3 GHz and its harmonics, the cables are shunted with a 50 Ω resistor. The VNA generates a 0-dBm signal at the resonance frequency in the GHz range, which incident from the probe to the sample. This power level is selected to provide an adequate signal-to-noise ratio (SNR) while minimizing sample destruction. A scanning frequency is chosen to maximize image contrast because the higher the frequency, the higher the sensitivity to small capacitances [2]. The VNA detects the signal reflected from the sample following its near-field interaction with the probe and records the reflection coefficient S_{11}. The intermediate frequency bandwidth of the VNA is set to 500 Hz, balancing SNR and scan rate. Under these conditions, a maximum 15 μm × 15 μm area can be scanned at a resolution of 256 × 256 pixels in approximately 4 min, corresponding to a scan rate of 200 pixels/s. During the same scan, SMM and AFM signals are simultaneously detected and recorded.

C. Traditional SMM Calibration

The measured S_{11} is converted to the probe-sample interaction admittance Y by one-port *in situ* calibration [1], [4]. The calibration is based on measuring S_{11} as the probe approaches the bare substrate between the SnSe flakes, while measuring the probe-sample capacitance C using the AFM in the mode of electrostatic force microscopy. By acquiring both $S_{11}(z)$ and $C(z)$ as functions of the probe-sample distance z, the error-correction coefficients e_{00}, e_{01}, and e_{11} are extracted for converting S_{11} to Y. For a given frequency with measured S11,m, the conversion into the impedance plane is the following [1]:

$$S_{11,m} = e_{00} + e_{01}\frac{S_{11,a}}{1 - e_{11}S_{11,a}} \quad (1)$$

where

$$S_{11,a} = \frac{Z_{in} - Z_{ref}}{Z_{in} + Z_{ref}} \quad (2)$$

Additionally, the probe geometry, such as the tip radius and the cone angle/height of the probe body, is extracted by fitting $C(z)$ curves with simulated probe characteristics [1].

After S_{11} is converted to Y, it is used to extract the conductivity of SnSe flakes using a simple equivalent circuit model validated by numerical simulations [9]. To this end, three-dimensional finite-element electromagnetic simulations are performed using the COMSOL AC/DC module.

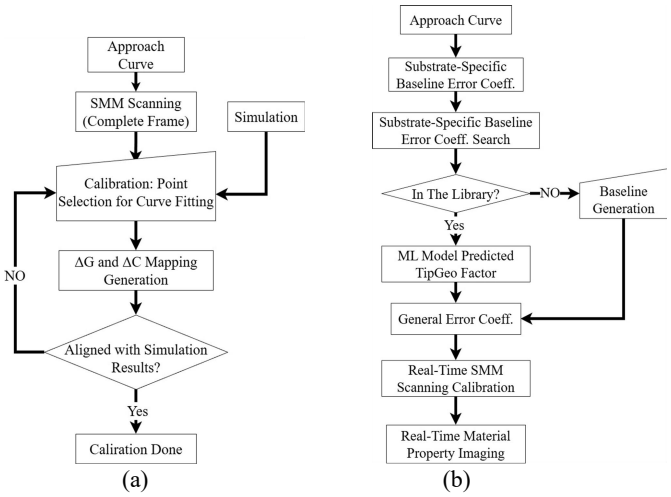


Fig. 2. Flowcharts of the calibration process: (a) manual calibration, which needs to wait for the completion of scanning, and (b) ML-assisted calibration, which can calibrate in real time.

D. Substrate-Reference Split-Calibration

The traditional calibration (Fig. 2a) is achieved via a three-term error model; however, in the near-field region, the error terms are highly dependent on the dynamic geometry of the probe tip, which degrades during scanning. To address this, and shorten the overall calibration time and complexity, we propose this split-calibration architecture (Fig. 2b) that

decouples static environmental parasitics from dynamic geometric variations.

The first step of the split-calibration process is to determine the static baseline error coefficients ($e_{00}^{base}, e_{01}^{base}, e_{11}^{base}$) associated with the specific substrate material (e.g., SiO_2/Si^{++}). These coefficients account for all static signal path contributions, including cable losses, connectors, and the large background stray capacitance of the cantilever body, which remains constant for a given substrate. To extract these baseline terms, we performed a far-field calibration by acquiring an experimental approach curve on the bare region of the exposed substrate between SnSe samples. Then following the same procedure as the traditional calibration process, this measured $C(z)$ curve is then line-fitted to the theoretical approach curve derived from COMSOL simulation, which represents the ideal tip-substrate interaction, to eventually obtain the baseline error coefficient set. This process is repeated for N approach curves taken at different locations and frequencies on the exposed substrates from different batches to account for any kind of inhomogeneities. We then compute the root mean square (RMS)-averaged values to identify a robustly defined set of static error coefficients.

Here we define the total error network as a transformation of static baseline error coefficients by a dynamic tip factor as follows:

$$\begin{bmatrix} e_{00} \\ e_{01} \\ e_{11} \end{bmatrix} = \begin{bmatrix} e_{00}^{base} \\ e_{01}^{base} \\ e_{11}^{base} \end{bmatrix} \odot \begin{bmatrix} G_{00}^{tip} \\ G_{01}^{tip} \\ G_{11}^{tip} \end{bmatrix} \tag{4}$$

Therefore, Eq. (1) has become:

$$S_{11,m} = (e_{00}^{base} \cdot G_{00}^{tip}) + (e_{01}^{base} \cdot G_{01}^{tip}) \frac{S_{11,a}}{1 - (e_{11}^{base} \cdot G_{11}^{tip}) S_{11,a}} \tag{5}$$

Here, the ML model learns and predicts the tip geometry factor set $[G_{00}^{tip} \quad G_{01}^{tip} \quad G_{11}^{tip}]^T$ to accelerate the overall calibration process with prior confirmed baseline error coefficients, which make real-time material property imaging capable.

E. TabPFN for Tip Geometry Factor Prediction

The sensitivity of the SMM calibration process necessitates extreme precision in the three error coefficients predictions. After many attempts, we found that the error coefficients in Eq. (5) must be accurate to at least the 4th decimal place, even minor deviations propagate non-linearly, leading to gross errors in the admittance extraction. Traditional lightweight models such as Random Forest or Multi-Layer Perceptrons (MLP) struggle to achieve this level of high-fidelity regression on complex, non-linear inverse problems, often overfitting to synthetic artifacts.

Therefore, we chose to use TabPFN (Tabular Prior-Data Fitted Network) which is a pre-trained transformer-based model for tabular dataset prediction via in-context learning [13] . To handle the multi-output regression task, we implemented a regressor chain architecture [14] and to emphasize the dependency among targets we also employed Gaussian Quantile Transformation [15] which can make sure the targets are predicted sequentially in a fixed chain order for their dependency learning.

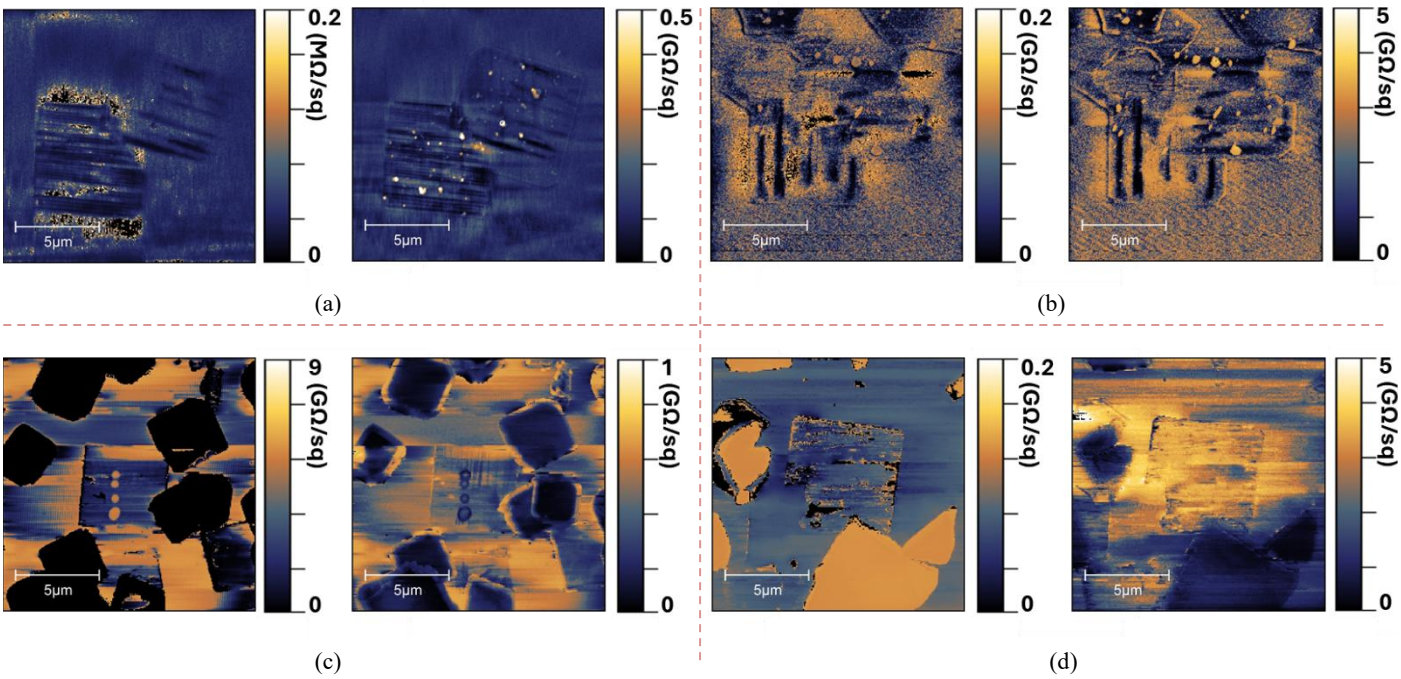


Fig. 3. Sheet Resistance Mappings: Manually calibrated (left) and DL-assisted split-calibrated (right) of four SnSe flakes on different substrates. On SiO_2/Si^{++} substrate at 15.70GHz with thicknesses 2.4nm(a) and 2.2nm(b); on Si^{++} substrate at 15.76GHz with thicknesses 7.27nm(c) and 51nm(d).

III. Results

To evaluate the capability of the proposed ML-assisted split calibration framework, we performed quantitative imaging [sheet resistance (R_{sh}) imaging] on SnSe flakes with varying thicknesses on two different substrates. Fig.3 presents a comprehensive comparison of the R_{sh} maps obtained via manual calibration versus the ML-assisted split-calibration. The results demonstrate the model's ability to consistently infer the tip geometry factor across diverse substrate environments and sample thicknesses. Furthermore, the ML-assisted maps reveal greater detailed features that are completely obscured in the manual calibration, which highlights the superior feature resolution of the DL approach. While the extreme values and relative trends are consistent between both methods, there still exists a systematic offset of one to two orders of magnitude difference observed in the ML-assisted calibrated R_{sh} maps. This difference is primarily attributed to the limited size of the training datasets. We anticipate that expanding the training dataset with more diverse experimental ground-truth samples will bridge this quantitative gap in the later iterations.

IV. Conclusion

This work introduced a novel machine-learning-assisted (TabPFN-based regressor chain) substrate-reference-calibration framework that will enable real-time material property imaging in SMM bypassing a sophisticated and time-consuming manual calibration process by decoupling the static environmental parasitics from the dynamic variations in the probe tip geometry.

By transforming SMM from a specialized niche imaging technique into a robust, high-throughput quantitative metrology tool, this work significantly shows the great potential of lowering the barrier to entry for non-expert users. Future development will focus on increasing accuracy to more decimal places by expanding the training dataset and creating a comprehensive universal real-time imaging suite for the broader materials science community.

Acknowledgment

This work was supported in part by in part by SUPREME, one of the seven centers sponsored by the Semiconductor Research Corporation and the U.S. Defense Advanced Projects Agency through the Joint University Microelectronics Program 2.0 under Contract 2023-JU-3137 This work was performed in part at the Cornell NanoScale Facility, an NNCI member supported by NSF Grant NNCI-2025233.

References

[1] G. Gramse, M. Kasper, L. Fumagalli, G. Gomila, P. Hinterdorfer, and F. Kienberger, "Calibrated complex impedance and permittivity measurements with scanning microwave microscopy," *Nanotechnol.*, vol. 25, no. 14, p. 145703, Mar. 2014.

[2] M. Farina and J. C. M. Hwang, "Scanning microwave microscopy for biological applications: Introducing the state of the art and inverted SMM," *IEEE Microw. Mag.*, vol. 21, no. 10, pp. 52–59, Oct. 2020.

[3] L. Zheng, L. Shao, M. Loncar, and K. Lai, "Imaging acoustic waves by microwave microscopy: Microwave impedance microscopy for visualizing gigahertz acoustic waves," *IEEE Microw. Mag.*, vol. 21, no. 10, pp. 60–71, Oct. 2020.

[4] M. Farina, D. Mencarelli, A. Di Donato, G. Venanzoni and A. Morini,, "Calibration protocol for broadband near-field microwave microscopy," *IEEE Trans. Microw. Theory Techn.*, vol. 59, no. 10, pp. 2769–2776, Oct. 2011.

[5] M. Farina, X. Jin, G. Fabi, E. Pavoni, A. Di Donato, D. Mencarelli, A. Morini, F. Piacenza, R. Al Hadi, Y. Zhao, T. Pietrangelo, X. Cheng, and J. C. M. Hwang, "Inverted scanning microwave microscope for in vitro imaging and characterization of biological cells," *Appl. Phys. Lett.*, vol. 114, no. 9, p. 093703, Mar. 2019.

[6] R. C. Chintala, "Scanning microwave impedance microscopy: Room-temperature and low-temperature applications for device and material characterization," *IEEE Microw. Mag.*, vol. 21, no. 10, pp. 22–35, Oct. 2020.

[7] S. Berweger, T. M. Wallis, and P. Kabos, "Nanoelectronic characterization: Using near-field microwave microscopy for nanotechnological research," *IEEE Microw. Mag.*, vol. 21, no. 10, pp. 36–51, Oct. 2020.

[8] A. Tselev, "Near-field microwave microscopy: Subsurface imaging for in situ characterization," *IEEE Microw. Mag.*, vol. 21, no. 10, pp. 72–86, Oct. 2020.

[9] X. Wang, K. Nomoto, G. Fabi, M. Farina, D. Jena, H. G. Xing, and J. C. M. Hwang, "Quantitative scanning microwave microscopy for transfer characteristics of GaN high-electron-mobility transistors," *IEEE Trans. Microw. Theory Techn.*, vol. 73, no. 3, pp. 1573–1580, Mar. 2025.

[10] X. Wang, K. Nomoto, G. Fabi, R. Al Hadi, M. Farina, D. Jena, H. G. Xing, and J. C. M. Hwang, "Inverted scanning microwave microscopy of GaN/AlN high-electron mobility transistors," in *2024 103rd ARFTG Microwave Measurement Conference (ARFTG)*, 2024, pp. 1–4.

[11] Y. Zhang, X. Wang, J. C. M. Hwang, N. Mao, P. Wang, and J. Kong, "Characterization of in-plane polarization domains in 2D SnSe by scanning microwave microscopy," in *2025 104th ARFTG Microwave Measurement Symposium (ARFTG)*, 2025, pp. 1–4.

[12] X. Jin, J. C. M. Hwang, D. Mencarelli, L. Pierantoni, and M. Farina, "Nano probing for microwave engineers: Calculating probe-sample capacitance and charge distribution of a near-field scanning microwave microscope on a nanoscale," IEEE Microw. Mag., vol. 18, no. 1, pp. 71–75, Jan. 2017.

[13] M.-H. Chiu, X. Ji, T. Zhang, N. Mao, Y. Luo, C. Shi, X. Zheng, H. Liu, Y. Han, W. L. Wilson, Z. Luo, V. Tung, and J. Kong, "Growth of large-sized 2D ultrathin SnSe crystals with in-plane ferroelectricity," *Adv. Electron. Mater.*, vol. 9, no. 3, p. 2201031, Mar. 2023.

[14] P. García, J. de Curtò, I. de Zarzà, J. C. Cano, and C. T. Calafate, "Foundation models for cybersecurity: A comprehensive multi-modal evaluation of TabPFN and TabICL for tabular intrusion detection," Electronics, vol. 14, no. 19, p. 3792, Sep. 2025.

[15] E. Spyromitros-Xioufis, G. Tsoumakas, W. Groves, and I. Vlahavas, "Multi-target regression via input space expansion: Treating targets as inputs," *Mach. Learn.*, vol. 104, no. 1, pp. 55–98, Jul. 2016.

[16] F. Pedregosa *et al.*, "Scikit-learn: Machine learning in Python," *J. Mach. Learn. Res.*, vol. 12, pp. 2825–2830, Oct. 2011.